

Ab-initio insights into the pressure dependent physical properties and possible high- T_c superconductivity in monoclinic and orthorhombic MgVH₆

Md. Ashrafal Alam^{1,2}, F. Parvin², S. H. Naqib^{2*}

¹Department of Physics, Mawlana Bhashani Science and Technology University, Santosh, Tangail 1902, Bangladesh

²Department of Physics, University of Rajshahi, Rajshahi 6205, Bangladesh

*Corresponding author; Email: salehnaqib@yahoo.com

Abstract

Here we have used the density functional theory (DFT) with the GGA-PBE approximation to investigate the structural, mechanical, electronic, hardness, thermal, superconductivity and optoelectronic properties under pressure for monoclinic ($P2_1/m$) and orthorhombic ($Pmn2_1$) structures of MgVH₆. We have studied optical properties of $P2_1/m$ phase at 0 GPa and $Pmn2_1$ phase at 100 GPa only (considering phase stability). Both of the phases of MgVH₆ are thermodynamically stable. $P2_1/m$ phase is mechanically stable but $Pmn2_1$ is mechanically unstable in our calculations for the pressures considered. Monoclinic ($P2_1/m$) is ductile in nature, on the other hand, orthorhombic ($Pmn2_1$) is brittle in nature at 100 GPa and becomes ductile for pressures in the range from 125 GPa to 200 GPa. Hardness calculations indicate superhard character of orthorhombic ($Pmn2_1$) structure at 100 GPa. The melting temperature of orthorhombic crystal is very high. This also agrees with the bulk modulus, Debye temperature, and hardness calculations. We have calculated theoretically the superconducting transition temperature T_c at different pressures only for the orthorhombic ($Pmn2_1$) structure following a previous study. The estimated values of transition temperatures are within 104.7 K to 26.1 K in the pressure range from 100 GPa to 200 GPa. MgVH₆, in both the structures, are elastically and optically anisotropic.

Keywords: Ternary hydride superconductors; DFT calculations; Elastic properties; Optoelectronic properties; Thermophysical properties

1. Introduction

Anion of hydrogen is known as hydride. Usually this is a compound in which one or more hydrogen atom(s) is(are) present. According to Gibb a metal-to-hydrogen bond known as hydride while Blackledge defined hydride as a binary combination of hydrogen and a metal or

metalloid [1]. On the other hand, according to the bonding nature, hydrides can be classified into four categories: (i) ionic hydride, (ii) covalent hydride, (iii) metallic hydride, and (iv) van der waals hydride [1]. Hydrogen can also be stored in three different phases; as gas, as liquid, and as solid. In solid hydrogen can be stored as chemical or physical combination with metals such as Li, Be, Na, Mg, B and Al, form a large variety of metal–hydrogen compounds and complex hydrides such as Na_3AlH_6 , Mg_2NiH_4 [2]. There are various applications of hydrogen storage systems such as nickel-metal used as hydride batteries and metal hydrides (M-H_n) used as thermal storage for off-board storage [3]. Hydrogen-storage densities in metal hydrides (e.g., MgH_2) can be 6.5 H atoms/ cm^3 while in gas it can be 0.99 H atoms/ cm^3 and in liquid 4.2 H atoms/ cm^3 [4]. VH_2 in the solid state contains 3.8 wt% hydrogen [5]. Metal hydride storage in solid is a better option than the gas or liquid storage system. At the same time, reversible hydrogen storage system with cyclic stability is very important. But the resistance of metal hydrides to impurities is one of the critical issues for on-board applications in order to maintain performance over the lifetime of the material [6,7].

Catalysis is also one of the serious factors in the improvement of hydrogen adsorption kinetics in metal hydride systems that enable dissociation of hydrogen molecules [8]. Palladium (Pd) is a good catalyst for hydrogen dissociation reaction [9]. Gennari et al., [10] used Pd, nickel (Ni), and germanium (Ge) as catalysts of hydrogenation kinetics. Hydrogen capacity can be increased up to 5.8 wt% using vanadium (V) as a catalyst [11].

Metal hydrides have attracted wide attention for not only as hydrogen (H) energy storage systems but also as potential high-temperature superconductors. For example, a number of H-rich binary compounds have shown superconductivity with very high superconducting transition temperature (T_c) under pressure e.g., 235 K for CaH_6 [12], 64 K for GeH_4 [13], 82 K for LiH_6 [14], 70 K for KH_6 [15], 38 K for BeH_2 [16] and so on [17-21]. H_3S is a remarkably high superconductivity with a superconducting T_c of 203 K at 200 GPa [22]. Transition metal hydrides are also interesting in the search for potential superconductors with high a T_c . For example, PdH at ambient pressure has a superconducting critical temperature of approximately 9 K with an unusual isotope effect [23]. Among the transition metals, V exhibits a transition temperature which increases from 5 K at 0 GPa to 17 K at 120 GPa [24-26].

Moreover, there are some predicted ternary hydrides with good superconducting properties under pressure such as ScCaH_8 and ScCaH_{12} with the corresponding $T_c \sim 212$ K and ~ 182 K, respectively, at 200 GPa [27]. ScYH_6 has $T_c \sim 32.110$ K to 52.907 K in the pressure range 0-200 GPa [28] and H_3SXe with a T_c of 89 K at 240 GPa [29]. The Mg based ternary hydrides are also investigated with predicted a MgGeH_6 T_c up to 67 K at 200 GPa [30]. The predicted superconducting critical temperature of CaYH_{12} 258 K at 200 GPa [31]. Besides, for LaSH_6 the estimated superconducting transition temperature is 35 K at 300 GPa [32], for MgSiH_6 , $T_c \sim 63$ K at 250 GPa [33], for MgScH_6 , $T_c \sim 41$ K at 100 GPa [34] and for MgVH_6 , $T_c \sim 27.6$ K at 150 GPa [35].

In general, Mg based hydrides have good-quality functional properties, such as heat-resistance, reversibility and recyclability. Among the Mg based hydrides MgH_2 is a promising material in solid-state due to its high storage capacity (7.6 wt% H_2), the availability, lower costs, crystal structure and superconductivity [35-38]. There are various Mg-H binary systems with predicted high temperature superconductivity at high pressures such as MgH_6 ($T_c = 260$ K) at 300 GPa [39], MgH_{12} ($T_c = 60$ K) at 140 GPa [40]. Sun et al. [41] introduce extra electron in Mg-H system to tune the superconducting transition temperature. It was suggested by J. W. Arblaster that V-H systems should have excellent superconducting transition temperature at ambient pressure [42, 43]. Estimated T_c of VH_5 is 24.5 K at 300 GPa [44] and for VH_8 it is 71.4 K at 200 GPa [45]. All these studies suggest that superconductivity of the binary Mg-H system may also be tuned by incorporating vanadium in the compound. Very recently, the structures of MgVH_6 were predicted by using the Crystal structure Analysis by Particle Swarm Optimization (CALYPSO) [46, 47]. Several phases such as $P2_1/m$, $C2/m$, $Pmn2_1$, $Cmc2_1$, $Cmcm$, and $P4/mmm$ were predicted for ternary MgVH_6 compound at ambient and under different pressures [36]. Previous studies focused on the crystal structure, elastic properties, phase transition, electronic structures, and superconductivity to a limited extent of the ternary Mg-V hydrides at different pressures [36]. In this work we are inclined to address the structural, elastic, electronic, thermal, superconducting, and optical properties of MgVH_6 in two different structures at different pressures in detail using the density functional theory (DFT) based ab-initio methodology.

2. Computational scheme

For geometry optimization plane wave pseudopotential [48] method was implemented in the CASTEP code [49]. Generalized gradient approximation (GGA) with PBE functional [50] was used for the electronic exchange-correlation terms. Ultrasoft pseudopotential was used for the calculations of electron-ion interactions [51]. Plane-wave cutoff of energy 380 eV was used throughout the calculations and the BFGS algorithm was used to minimize the total energy and internal forces [52]. Size of the Monkhorst–Pack grid [53] was $4 \times 8 \times 5$ for $P2_1/m$ phase and $5 \times 5 \times 5$ for $Pmn2_1$ phase for sampling of the first Brillouin zone (BZ). The quality of convergence tolerance for optimizing the geometry was set as: difference in total energy 5×10^{-6} eV/atom, maximum force 0.01 eV/Å, maximum stress 0.02 GPa, maximum displacement 0.001 Å, and self-consistent field tolerance within 5×10^{-4} eV/atom. The valence electron configurations were as follows: Mg[$2p^6 3s^2$], V[$3s^2 3p^6 3d^3 4s^2$], H[$1s^1$]. The elastic constants were determined using the stress-strain module in CASTEP. The optical constants were calculated from the matrix element of optical transition of electrons from the valence band to the conduction band. Thermophysical parameters were computed from the elastic constants and moduli.

3. Results and analysis

3.1 Structure and stability

The crystal structures of monoclinic and orthorhombic crystal system belonging to the space groups $P2_1/m$ and $Pmn2_1$, respectively, are shown in Fig. 1. In Fig. 1 we represent the crystal structure at 0 GPa and 100 GPa of (a) monoclinic and (b) orthorhombic structures of MgVH₆, respectively. For both the monoclinic and orthorhombic crystal structures the unit cell contains two formula units with sixteen atoms in total. The calculated lattice parameters are listed in Table 1 with the previous values for comparison. The optimized lattice parameters are consistent with the previous work for both of the structure. In this work, we have calculated the cohesive energy per atom using the equation [54-56]

$$E_{coh} = \frac{E_{Mg} + E_V + 6E_H - E_{MgVH_6}}{8} \quad (1)$$

Where, E_{MgVH_6} is total energy per formula unit of MgVH₆ and E_{Mg} , E_V and E_H are total energy of single Mg, V and H atoms, respectively. From Table 1 it is found that the values of cohesive

energy per atom are positive for MgVH_6 , which indicate that two phases $P2_1/m$ and $Pmn2_1$ of MgVH_6 are thermodynamically stable. The values of lattice parameters a and c decrease at a faster rate than b with pressure indicating that a and c directions of the $P2_1/m$ crystal are easily compressible than the b direction under pressure. For the $Pmn2_1$ structure the pressure dependences of a , b , and c are similar with significantly different behavior occurring at pressures above 170 GPa. This is an indication of structural instability.

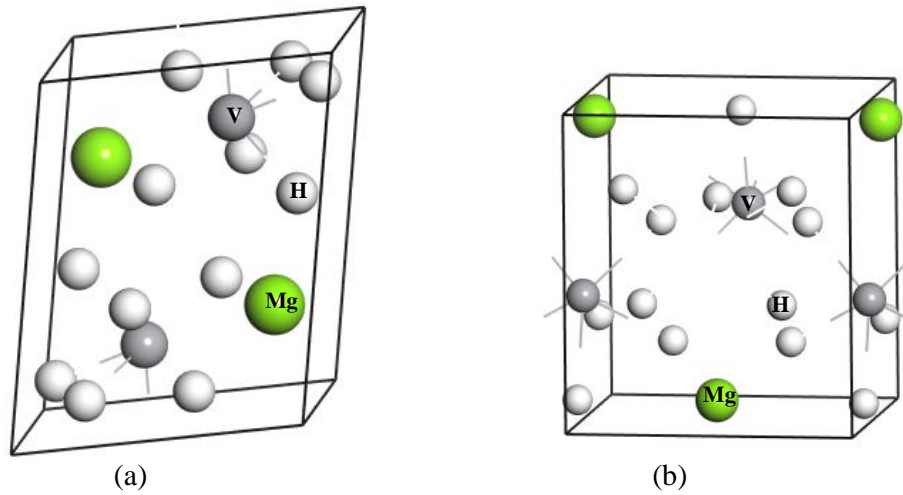
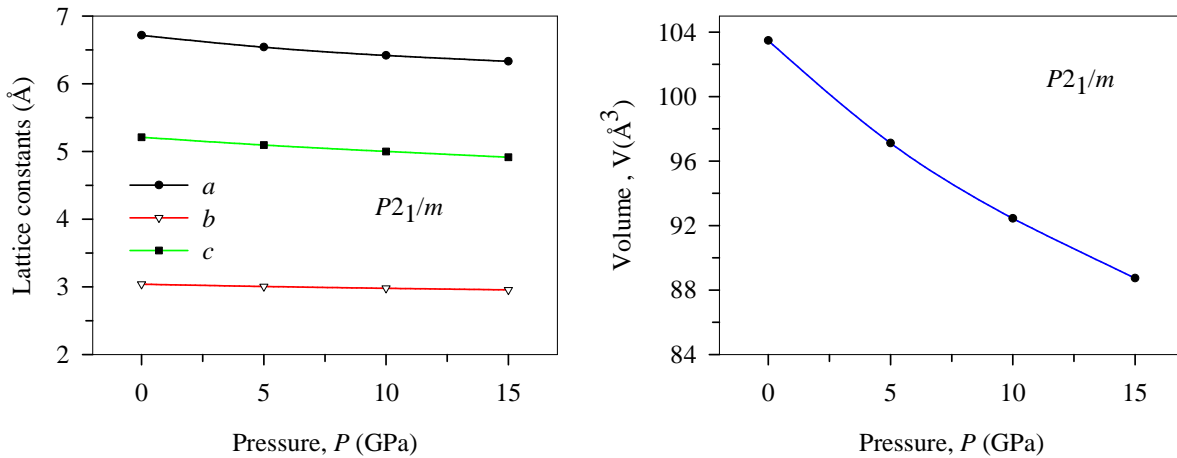


Figure 1: Crystal structures of (a) $P2_1/m$ and (b) $Pmn2_1$ MgVH_6 .



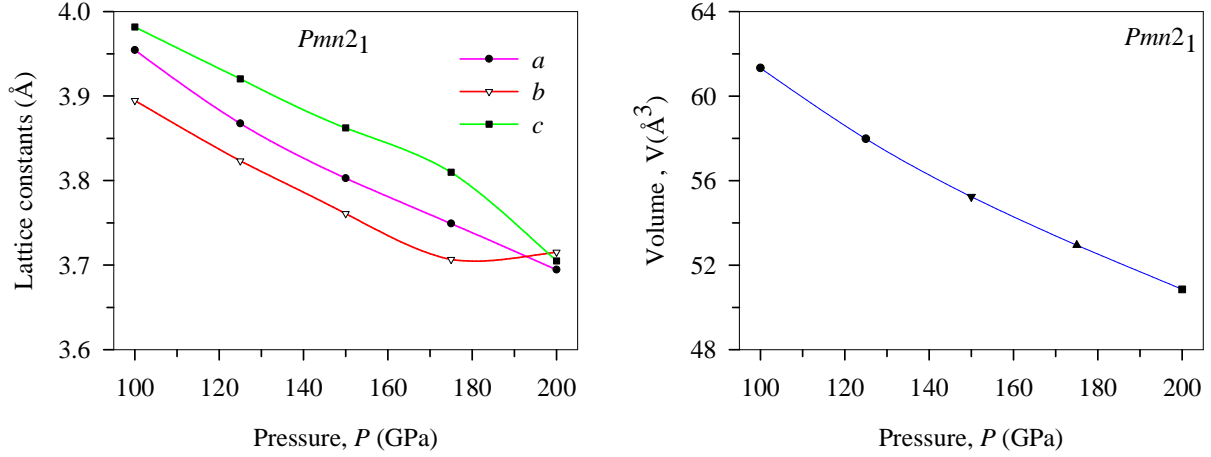


Figure 2: Lattice parameters under pressure of $MgVH_6$ in two different structures.

Table 1. The calculated lattice parameters a (Å), b (Å), c (Å), cell volume V (Å³), and cohesive energy E_{coh} (eV/atom) of $MgVH_6$ in different structures.

Space group	Crystal structure	Pressure P (GPa)	a	b	c	V	E_{coh}	Ref.
$P2_1/m$	Monoclinic	0	6.65870	3.02040	5.13840	-	-	[36]
		0	6.71398	3.03794	5.20925	103.47	3.85	[This]
		5	6.53858	3.00484	5.09337	97.11	3.84	
		10	6.41669	2.97763	4.99983	92.44	3.83	
		15	6.32944	2.95462	4.91356	88.73	3.81	
		25	6.19790	2.89270	4.75360	-	-	[36]
$Pmn2_1$	Orthorhombic	100	3.9544	3.8947	3.9817	61.32	3.28	[This]
		125	3.8676	3.8233	3.9204	57.97	3.14	
		150	3.8028	3.7608	3.8622	55.24	2.99	
		150	3.8108	3.7582	3.8433	-	-	[36]
		175	3.7490	3.7066	3.8099	52.94	2.85	[This]
		200	3.6945	3.7154	3.7049	50.85	2.69	
		200	3.6943	3.6527	3.7694	-		[36]

3.2 Elastic properties

3.2.1 Single crystal elastic constants

For the monoclinic crystal structure, there are thirteen independent elastic constants: C_{11} , C_{22} , C_{33} , C_{44} , C_{55} , C_{66} , C_{12} , C_{13} , C_{15} , C_{23} , C_{25} , C_{35} and C_{46} . For the orthorhombic crystal structure there are nine independent elastic constants: C_{11} , C_{22} , C_{33} , C_{44} , C_{55} , C_{66} , C_{12} , C_{13} and C_{23} . The computed independent elastic constants are listed in Table 2. From Table 2 it is observed that most of the elastic constants increase with increasing pressure for both of the phases except C_{15} , C_{25} , C_{35} , C_{46} for the monoclinic and C_{22} , C_{44} for the orthorhombic structure. The negative values of elastic constants imply that the optimized geometries are not completely relaxed and internal

strains are present within the crystals. The largest values of the elastic constants are found for C_{11} , C_{22} , C_{33} for both of the structures indicating that deformation resistances along the a -, b - and c -axis are very strong. According to Liu, Q. J. et al. [57] the mechanical stability conditions of monoclinic and orthorhombic crystals under pressure are as follows:

For the monoclinic structure:

$$C_{11} - P > 0, C_{22} - P > 0, C_{33} - P > 0, C_{44} - P > 0, C_{55} - P > 0, C_{66} - P > 0 \quad (2)$$

$$C_{11} + C_{22} + C_{33} + 2C_{12} + 2C_{13} + 2C_{23} + 3P > 0 \quad (3)$$

$$(C_{11} - P)(C_{33} - P) > C_{35}^2, (C_{44} - P)(C_{66} - P) > C_{46}^2, (C_{22} + C_{33} - 2C_{23} - 4P) > 0 \quad (4)$$

$$(C_{22} - P)[(C_{33} - P)(C_{55} - P) - C_{35}^2] + 2(C_{23} - P)C_{25}C_{35} > (C_{23} + P)^2(C_{55} - P) + C_{25}^2(C_{33} - P) \quad (5)$$

$$\begin{aligned} & 2C_{15}C_{25}[(C_{33} - P)(C_{12} + P) - (C_{13} + P)(C_{23} + P)] \\ & + 2C_{15}C_{35}[(C_{22} - P)(C_{13} + P) - (C_{12} + P)(C_{23} + P)] \\ & + 2C_{25}C_{35}[(C_{11} - P)(C_{12} + P) - (C_{12} + P)(C_{13} + P)] \\ & - C_{15}^2[(C_{22} - P)(C_{33} - P) - (C_{23} + P)^2] - C_{25}^2[(C_{11} - P)(C_{33} - P) - (C_{13} + P)^2] \\ & - C_{35}^2[(C_{11} - P)(C_{22} - P) - (C_{12} + P)^2] \\ & + (C_{55} - P)[(C_{13} - P)(C_{22} - P)(C_{33} - P) - (C_{11} - P)(C_{23} + P)^2] \\ & - (C_{22} - P)(C_{13} + P)^2 - (C_{33} - P)(C_{12} + P)^2 + 2(C_{12} + P)(C_{13} + P)(C_{23} + P) \\ & > 0 \end{aligned} \quad (6)$$

For the Orthorhombic structure:

$$C_{11} - P > 0, C_{22} - P > 0, C_{33} - P > 0, C_{44} - P > 0, C_{55} - P > 0, C_{66} - P > 0 \quad (7)$$

$$(C_{11} + C_{22} - 2C_{12} - 4P) > 0, (C_{11} + C_{33} - 2C_{13} - 4P) > 0, (C_{22} + C_{33} - 2C_{23} - 4P) > 0, (C_{11} + C_{22} + C_{33} + 2C_{12} + 2C_{13} + 2C_{23} + 3P) > 0 \quad (8)$$

Our calculated result shows that $P2_1/m$ phase satisfies all conditions under pressure so $P2_1/m$ phase is mechanically stable under pressures up to 15 GPa. On the other hand, $Pmn2_1$ phase is mechanically unstable because it does not satisfy all the stability conditions.

Table 2. Calculated single crystal elastic constants C_{ij} (GPa) for $MgVH_6$.

C_{ij}	Monoclinic ($P2_1/m$)				Orthorhombic ($Pmn2_1$)					Ref.
	Pressure, P (GPa)				Pressure, P (GPa)					
	0	5	10	15	100	125	150	175	200	
C_{12}	34.05	53.51	57.08	87.86	319.65	406.81	432.99 382.26	488.64	557.85 436.48	[This] [36]
C_{13}	50.86	73.44	94.24	114.39	375.27	413.40	483.18 321.99	533.54	597.46 418.99	[This] [36]
C_{15}	2.89	8.65	15.04	0.04						[This]
C_{23}	51.00	73.01	75.06	105.00	335.68	379.68	449.80	503.33	574.03	[This]

							376.62		436.01	[36]
C_{25}	0.60	0.85	2.36	-15.32						[This]
C_{35}	-0.21	13.14	27.48	20.67						
C_{46}	-4.89	-4.60	-2.92	-0.56						
C_{11}	100.91	129.36	160.96	187.27	543.70	624.08	757.90 513.36	860.94	955.83 695.30	[This] [36]
C_{22}	202.10	249.65	258.26	322.00	551.50	633.09	728.24 503.34	838.94	890.37 695.30	[This] [36]
C_{33}	100.28	131.18	155.87	174.87	614.29	649.56	767.22 584.92	851.96	949.79 714.71	[This] [36]
C_{44}	46.15	55.23	62.35	66.35	159.34	179.50	197.45 200.50	211.80	223.33 98.88	[This] [36]
C_{55}	28.85	35.74	41.30	47.86	-41.93	-98.20	103.17 249.05	157.98	228.81 98.88	[This] [36]
C_{66}	37.11	43.89	49.76	54.27	145.10	163.25	181.49 187.95	197.00	212.21 211.10	[This] [36]

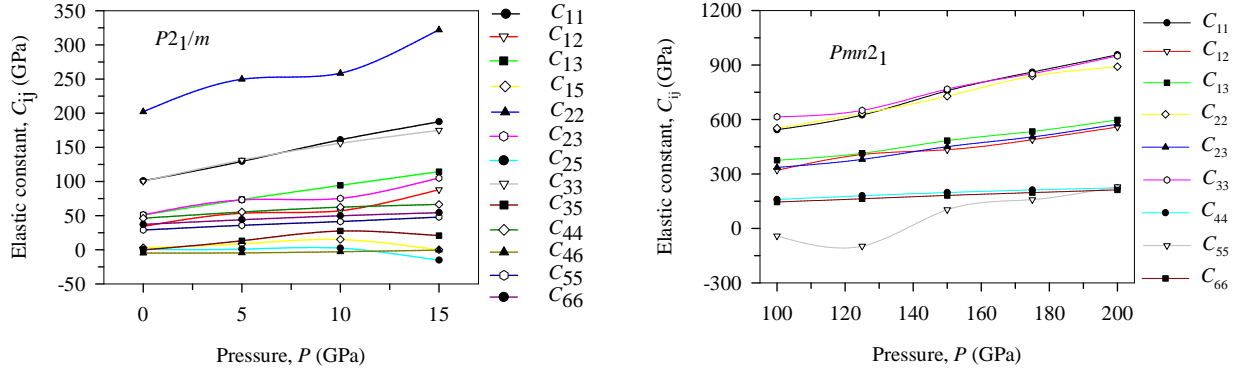


Figure 3: Single crystal elastic constants C_{ij} (GPa) under pressure of $MgVH_6$ compounds with different structures.

From Fig. 3 it is observed that the elastic constant C_{55} of $MgVH_6$ in the orthorhombic phase shows strongly nonmonotonic variation with pressure in the range from 100 GPa to 160 GPa. This observation might be linked with a possible structural instability as seen in Fig. 2 (for $Pmn2_1$ structure) at somewhat higher pressure.

3.2.2 Polycrystalline elastic properties

The polycrystalline elastic parameters such as Young's modulus, bulk modulus, shear modulus Poisson's ratio, Pugh's ratio, and machinability index are important indicators to evaluate the mechanical performance of a solid. As we know, Young's modulus represents the ability of a solid to counter uniaxial tension, shear modulus represents the resistance to shape changing plastic deformation, and bulk modulus can be used to characterize the resistance to change in the volume. The value of Young's modulus Y , shear modulus G , bulk modulus B are calculated of

monoclinic and orthorhombic structures for MgVH₆ by using the Voigt-Reuss-Hill (VRH) approximation [58-60].

Table 3. Calculated polycrystalline bulk modulus B (GPa), shear modulus G (GPa), Young's modulus Y (GPa), Pugh's ratio G/B , Poisson's ratio ν , and machinability index μ_m for MgVH₆.

Space group	Crystal structure	Pressure P (GPa)	B	G	Y	G/B	ν	μ_m	Ref.
$P2_1/m$	Monoclinic	0	72.45	37.73	96.44	0.52	0.28	1.57	[This]
		5	96.95	44.47	115.71	0.46	0.30	1.76	
		10	109.51	49.69	129.48	0.45	0.30	1.76	
		15	140.82	53.56	142.60	0.38	0.33	2.12	
$Pmn2_1$	Orthorhombic	100	417.19	391.84	895.25	0.94	0.142	2.62	[This]
		125	478.41	181.68	483.79	0.38	0.331	2.67	
		150	553.16	151.63	416.81	0.27	0.374	2.80	
		175	622.22	180.58	493.95	0.29	0.368	2.94	
		200	694.03	202.65	554.02	0.29	0.367	3.11	

The calculated values of polycrystalline elastic moduli, Pugh's ratio G/B , Poisson's ratio ν , machinability index μ_m are listed in Table 3. It can be seen from Table 3 and Fig. 4 that the values of Young's modulus, shear modulus, bulk modulus of monoclinic MgVH₆ structure increase with pressure which indicates the resistance to plastic deformation and uniaxial tension is enhanced up to 15 GPa. For orthogonal structure of MgVH₆ only the bulk modulus increases with pressure and the values of shear and Young's modulus are gradually decrease up to 150 GPa. This behavior is anomalous and once again points towards a tendency of structural instability. Sudden increase in the Poisson's ratio from 0.142 (at 100 GPa) to 0.331 (at 125 GPa) is another indication that there is a drastic change in the bonding characteristics in this pressure range. Above 150 GPa, these values increase which indicates the resistance to plastic deformation and uniaxial tension is enhanced from 150 GPa to 200 GPa for the orthorhombic MgVH₆.

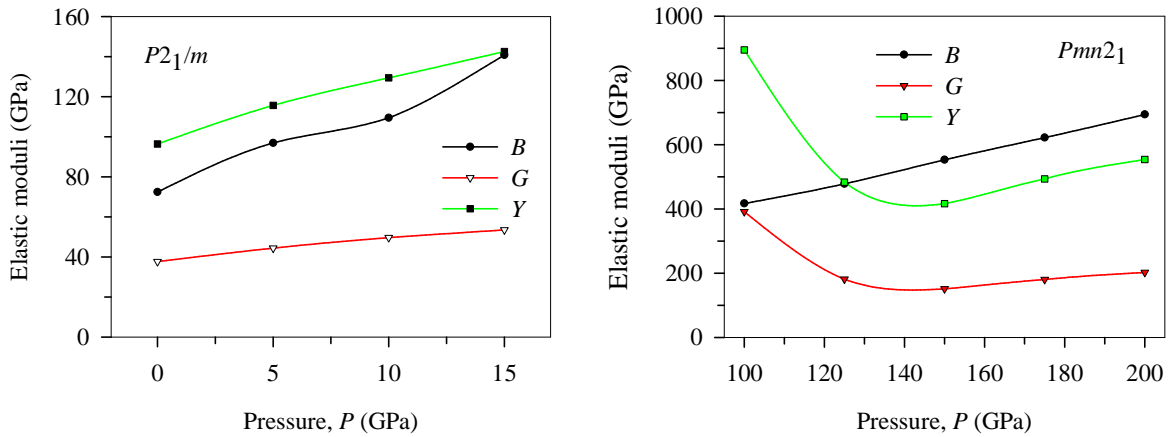


Figure 4: Polycrystalline elastic constant under pressure of MgVH₆ in the monoclinic and orthorhombic structures.

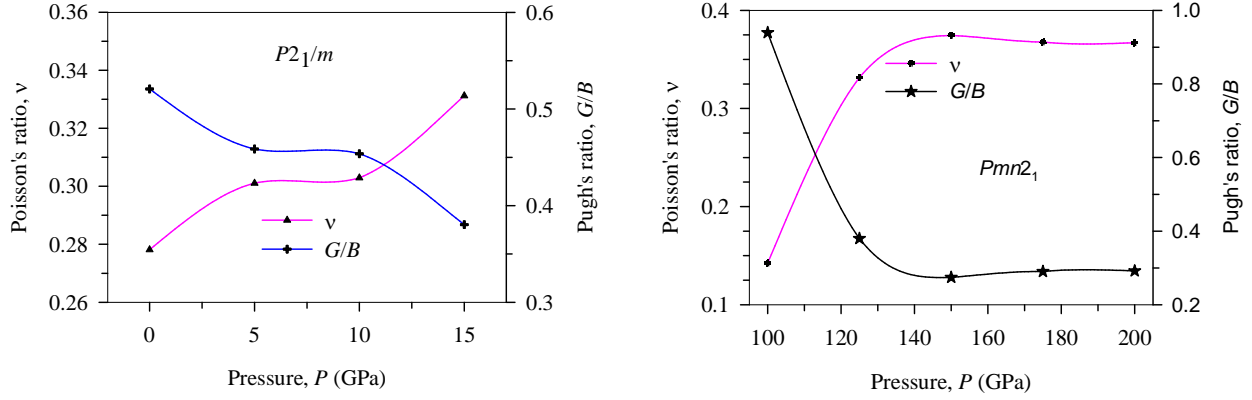


Figure 5: Poisson's ratio and Pugh's ratio under pressure of MgVH₆ in the monoclinic and orthorhombic structures.

The value of Poisson's ratio is obtained using the equation, $\nu = (3B - 2G)/(3B + G)$. This value indicates the ductile and brittle nature of a compound. According to Frantsevich [61], if $\nu > 0.26$ the solid should exhibit ductile nature otherwise it should be brittle. For the monoclinic structure ($P2_1/m$), the values of ν are greater than 0.26 which indicates the ductile nature of $P2_1/m$ phase of MgVH₆ for the pressures considered. Poisson's ratio and hence the degree of ductility increases with increasing pressure. On the other hand, for the $Pmn2_1$ phase, the value of ν is less than 0.26 at 100 GPa, and from 125 GPa to 200 GPa, ν is larger than 0.26. This indicates the brittle nature at 100 GPa and ductile nature in the pressure range from 125 GPa to 200 GPa. The Pugh's ratio (G/B) [63] is another parameter used to define ductile and brittle nature of a compound [62]. $G/B > 0.57$ indicates the brittle nature and otherwise ductility. From Table 3 it is observed that the Pugh's ratio indicates the same nature as the Poisson's ratio. Fig. 5 shows an anticorrelation between the Poisson's ratio and the Pugh's ratio.

3.3 Elastic anisotropy

Study of the elastic anisotropy is important to understand the direction dependent bonding characteristics and mechanical properties of solids. The shear anisotropy factors [63] obtained from our calculations are given in Table 4. These factors A_1 , A_2 , and A_3 must be one for an isotropic crystal, while any value except unity is a measure of the degree of elastic anisotropy possessed by the crystal. The factors A_1 , A_2 , and A_3 are computed from the expressions given follows:

$$A_1 = \frac{4C_{44}}{C_{11} + C_{33} - 2C_{13}}, A_2 = \frac{4C_{55}}{C_{22} + C_{33} - C_{23}}, A_3 = \frac{4C_{66}}{C_{11} + C_{22} - 2C_{12}} \quad (9)$$

Furthermore, A^B and A^G are the percentage anisotropies in compressibility and shear, respectively and A^U is the universal anisotropic factor. The zero values of A^B , A^G and A^U represent elastical isotropy of a crystal and non-zero values represent anisotropy [64, 65]. The

values of A^U , A^B , and A^G are also listed in Table 4. These anisotropy indices are calculated using the following equations:

$$A^B = \frac{B_V - B_R}{B_V + B_R}, A^G = \frac{G_V - G_R}{G_V + G_R} \text{ and } A^U = 5 \frac{G_V}{G_R} + \frac{B_V}{B_R} + 6 \geq 0 \quad (10)$$

Table 4. Calculated elastic anisotropic factors of MgVH₆.

Space group	Crystal structure	Pressure P (GPa)	A_1	A_2	A_3	A^U	A^B	A^G	Ref.
$P2_1/m$	Monoclinic	0	1.86	0.58	0.63	0.79	0.04	0.14	[This]
		5	1.94	0.61	0.65	0.86	0.04	0.15	
		10	1.94	0.63	0.65	1.02	0.04	0.19	
		15	1.99	0.67	0.65	1.14	0.02	0.22	
$Pmn2_1$	Orthorhombic	100	1.56	-0.34	1.27	-4.28	0.004	-0.75	[This]
		125	1.61	-0.75	1.47	-3.20	0.000	-0.47	
		150	1.41	0.69	1.17	0.27	0.001	0.03	
		175	1.31	0.92	1.09	0.07	0.001	0.01	
		200	1.26	1.32	1.16	0.07	0.001	0.01	

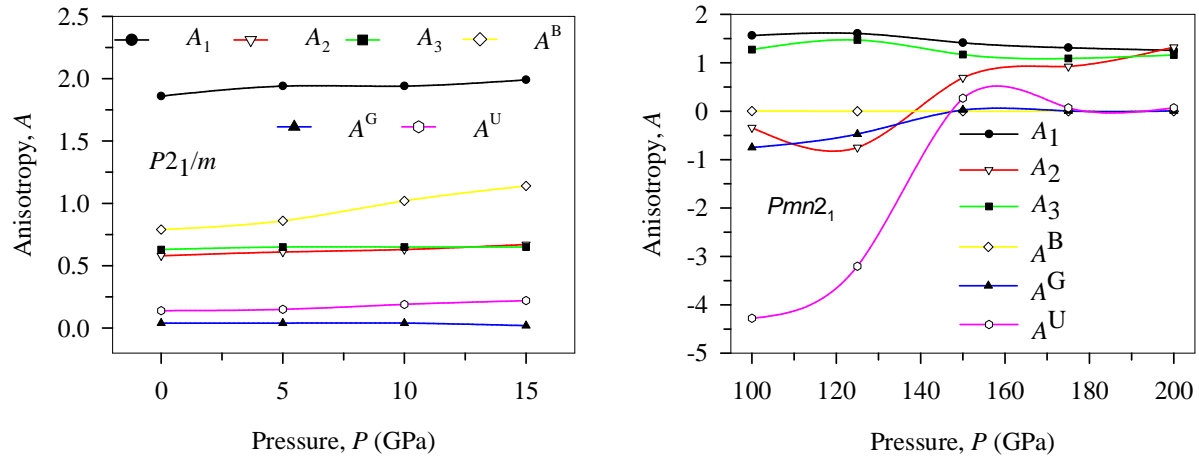


Figure 6: Anisotropy factors under pressure of MgVH₆ in the monoclinic and orthorhombic structures.

Table 4 (and Fig. 6) shows clearly that MgVH₆ in both monoclinic and orthorhombic structures are elastically anisotropic. These anisotropies are clear indications that atomic bonding strengths in different directions in the crystals are different. The negative values of A^U in the orthorhombic structure at 100 GPa and 125 GPa are indicative of structural instability.

3.4 Acoustic sound velocities

The sound velocities in a crystal are useful thermophysical parameter. They are closely related to the crystal stiffness and crystal density and determine the Debye temperature and thermal

conductivity to a large extent. Crystalline solids support both longitudinal and transverse modes of propagation of acoustic disturbances. The calculated values of Sound velocities (v_t , v_l and v_m) under pressure of MgVH₆ are listed in Table 5 using the following equations [66-68]:

$$v_t = \sqrt{\frac{G}{\rho}}, \quad v_l = \sqrt{\frac{3B + 4G}{3\rho}} \quad \text{and} \quad v_m = \left[\frac{1}{3} \left(\frac{2}{v_t^3} + \frac{1}{v_l^3} \right) \right]^{-\frac{1}{3}} \quad (11)$$

The computed values at different pressures are enlisted in Table 5 and shown in Fig. 7.

Table 5. Calculated density ρ (gm/cm³), transverse sound velocities v_t (km/s), longitudinal sound velocities v_l (km/s) and average sound velocities v_m (km/s) of MgVH₆.

Space group	Crystal structure	Pressure P (GPa)	ρ	v_t	v_l	v_m	Ref.
$P2_1/m$	Monoclinic	0	2.609	3.8026	6.8591	4.2359	[This]
		5	2.780	3.9997	7.4973	4.4682	
		10	2.920	4.1249	7.7581	4.6092	
		15	3.042	4.1956	8.3520	4.7054	
$Pmn2_1$	Orthorhombic	100	1.597	15.6657	24.2591	17.1933	[This]
		125	1.689	10.3713	20.6561	11.6318	
		150	1.773	9.2489	20.6426	10.4332	
		175	1.849	9.8814	21.6018	11.1365	
		200	1.925	10.2594	22.3790	11.5613	

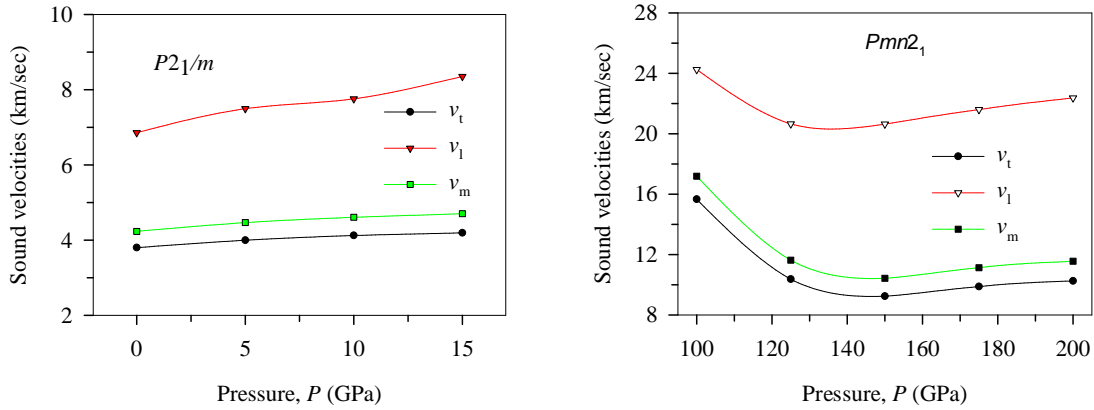


Figure 7: Sound velocities (v_t , v_l and v_m) under pressure of MgVH₆ in the monoclinic and orthorhombic structures.

From Fig. 7 [cf. Table 5] it is observed that for the $P2_1/m$ phase, all the sound velocities increase monotonously with pressure. For the $Pmn2_1$ phase, v_t decreases in the pressure range from 100 GPa to 125 GPa and increases after 125 GPa with increase in the pressure. Sound velocity is

greatly enhanced in the orthorhombic phase. This is a consequence of the greatly enhanced stiffness of the MgVH_6 compound in the orthorhombic structure.

3.5 Hardness of MgVH_6

Hardness of a solid is used to assess both elastic and plastic behavior of the material under mechanical stress. This particular parameter determines the average bonding strength and stiffness of a solid. A variety of approaches are available to compute the hardness of a system. In this study we have calculated the hardness using the formalisms developed by Teter et al. [69], Tian et al. [70], and Chen et al. [71]. We have also calculated the micro hardness [72] of MgVH_6 at different pressures in the monoclinic and orthorhombic structures. The calculated values of hardness are presented in Table 6. The pressure dependent hardness values are also illustrated in Fig. 8.

Table 6. Hardness of MgVH_6 in the monoclinic and orthorhombic structures.

Space group	Crystal structure	Pressure P (GPa)	Hardness (GPa)				Ref.
			H_{Teter}	H_{Tian}	H_{Chen}	H_{micro}	
$P2_1/m$	Monoclinic	0	5.70	4.92	4.79	5.58	[This]
		5	6.71	4.64	4.40	5.90	
		10	7.50	4.95	4.79	6.53	
		15	8.09	4.10	3.62	6.03	
$Pmn2_1$	Orthorhombic	100	59.17	57.87	58.12	93.43	[This]
		125	27.43	9.71	10.51	20.41	
		150	22.90	5.47	5.30	12.69	
		175	27.27	6.69	6.83	15.93	
		200	30.60	7.32	7.59	17.97	

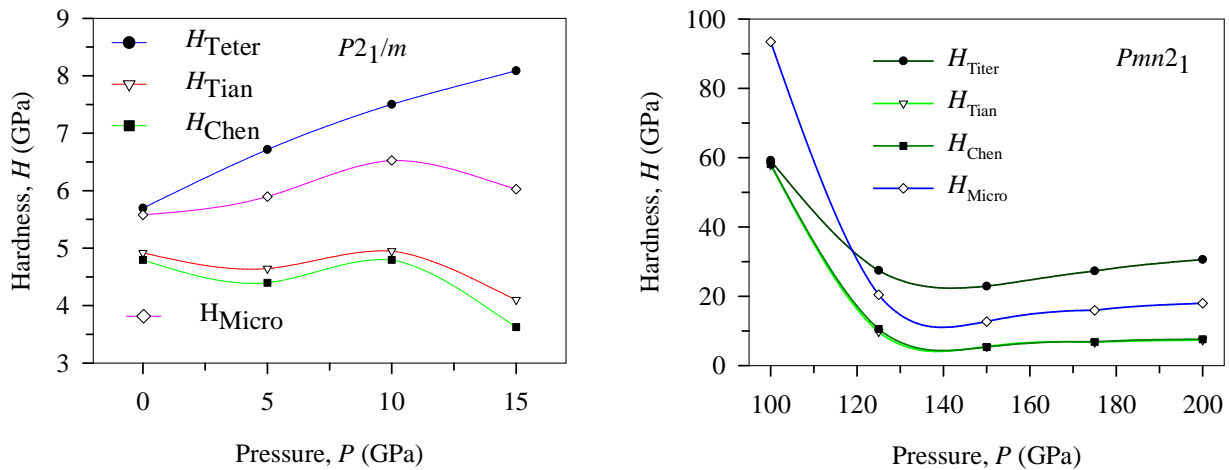


Figure 8: Hardness under pressure of MgVH_6 in the monoclinic and orthorhombic structures.

Fig. 8 shows that different formalisms result in different values of hardness. In the monoclinic phase Teter formalism yields the highest hardness. Overall the hardness of MgVH₆ in the monoclinic structure is moderate. At 100 GPa, MgVH₆ in the orthorhombic phase exhibits anomalously high hardness which falls sharply with increasing pressure. This is an indication of a drastic modification of pressure induced bonding strength in the orthorhombic phase. At high enough pressures both the structures are quite soft.

3.6 Thermodynamic properties

Debye temperature: The Debye temperature θ_D of a system is closely connected to many physical properties of solids such as specific heat, melting temperature, thermal conductivity, hardness, elastic constants, bonding strength, and sound velocity. The knowledge of θ_D provides information about the electron-phonon coupling and Cooper pairing mechanism of superconductivity. The Debye temperature calculated from the elastic constants is considered to be similar to that acquired from the specific heat measurements. Using the average sound velocity, the Debye temperature can be calculated by using the Anderson method [73] as follows:

$$\theta_D = \frac{h}{k_B} \left[\left(\frac{3n}{4\pi} \right) \frac{N_A \rho}{M} \right]^{1/3} v_m \quad (12)$$

where, h is Planck's constant, k_B is the Boltzmann's constant, V is the volume of unit cell, n is the number of atoms within a unit cell, and v_m is the average sound velocity. The computed results are disclosed in Table 7.

Minimum thermal conductivity: At temperatures above θ_D the thermal conductivity of a solid attains a minimum value known as the minimum thermal conductivity, κ_{min} . The calculated values of the minimum thermal conductivity are derived from the relation given by $\kappa_{min} = k_B v_m (V_a)^{-2/3}$ [74] and presented in Table 7.

Grüneisen parameter: The Grüneisen parameter γ is an important thermophysical quantity that links the vibrational properties with the structural ones. It is related to the expansion coefficient, bulk modulus, specific heat, and electron-phonon coupling in solids. The normal thermal expansion of solids due to anharmonicity of interatomic forces is understood from the Grüneisen constant as well. The relation between Grüneisen parameter and Poisson's ratio is as follows: $\gamma = \frac{3}{2} \frac{1+\nu}{2-3\nu}$ [75]. The calculated values of Grüneisen parameters at different pressures are presented in Table 7.

Melting temperature: Information on the melting temperature of a compound is very important for practical applications at different temperatures. High melting temperature of a compound has lower thermal expansion and high binding energy and vice versa. We have calculated the melting temperature T_m using the following equation [76]:

$$T_m = 354 + \frac{4.5(2C_{11} + C_{33})}{3} \quad (13)$$

The calculated values of melting temperatures of two phases of $P2_1/m$ and $Pmn2_1$ $MgVH_6$ are listed in Table 7. The melting temperatures of $Pmn2_1$ are very high at different pressures. This also agrees with the previously estimated bulk modulus, Debye temperature, and hardness. The melting temperature increases with the increase in the pressure for both the structures.

Thermal expansion coefficient: The thermal expansion coefficient (TEC) of a material is connected to many other physical properties, such as thermal conductivity, heat capacity, temperature variation of the energy band gap and electron effective mass. The thermal expansion coefficient of a material can be obtained using the following equation [67]:

$$\alpha = \frac{1.6 \times 10^{-3}}{G} \quad (14)$$

The relation between thermal expansion coefficient and the melting temperature can be approximated as $\alpha \approx 0.02/T_m$ [76]. From Table 7 it is observed that for $Pmn2_1$ has lower thermal expansion compared to $P2_1/m$.

Pressure variation of Debye temperature and the Grüneisen parameter are shown in Fig. 9.

Table 7. Grüneisen parameter γ , Debye temperature θ_D (K), thermal expansion coefficient α (K^{-1}), minimum thermal conductivity (W/m.K), and melting temperature T_m (K) of $MgVH_6$ in the monoclinic and orthorhombic structures.

Space group	Crystal structure	Pressure P (GPa)	γ	θ_D	α (10^{-5})	k_{min}	T_m	Ref.
$P2_1/m$	Monoclinic	0	1.64	676.25	4.24	1.01	807.14	[This]
		5	1.78	728.56	3.60	1.11	938.85	
		10	1.79	764.01	3.22	1.18	1070.70	
		15	1.98	790.70	2.99	1.24	1178.11	
$Pmn2_1$	Orthorhombic	100	1.09	2330.44	0.41	9.18	2906.54	[This]
		125	1.99	1606.44	0.88	6.45	3200.57	
		150	2.35	1464.29	1.06	5.97	3778.52	
		175	2.29	1585.24	0.89	6.56	4214.74	
		200	2.28	1667.94	0.79	7.00	4646.19	

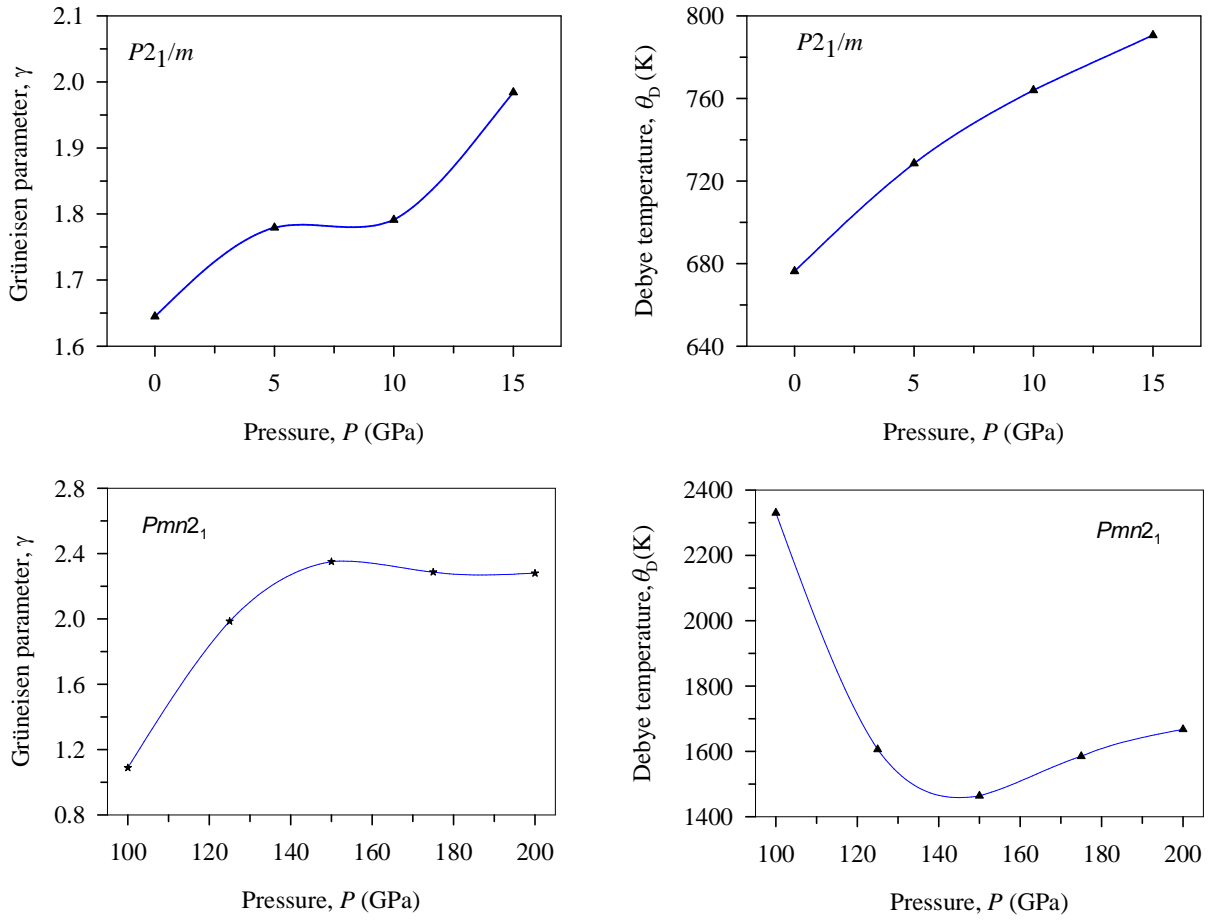


Figure 9: Grüneisen parameter and Debye temperature of MgVH_6 at different pressures.

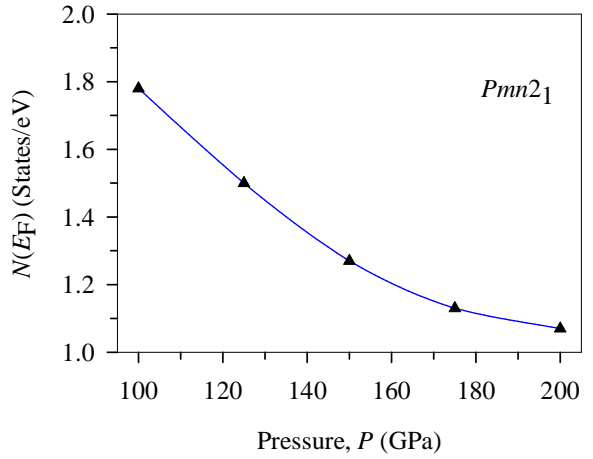
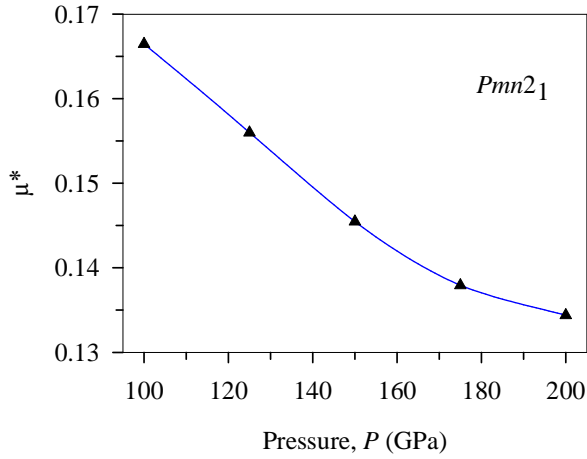
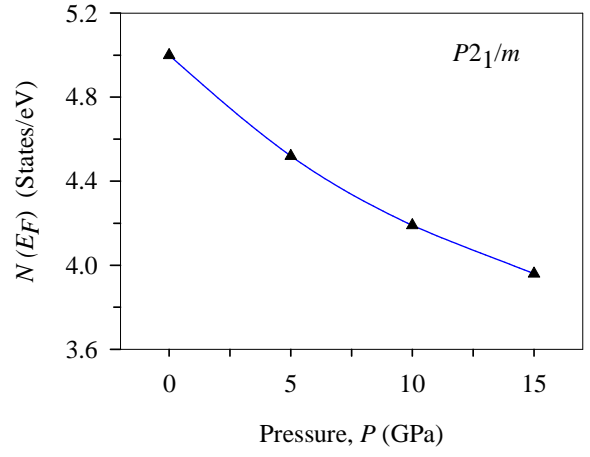
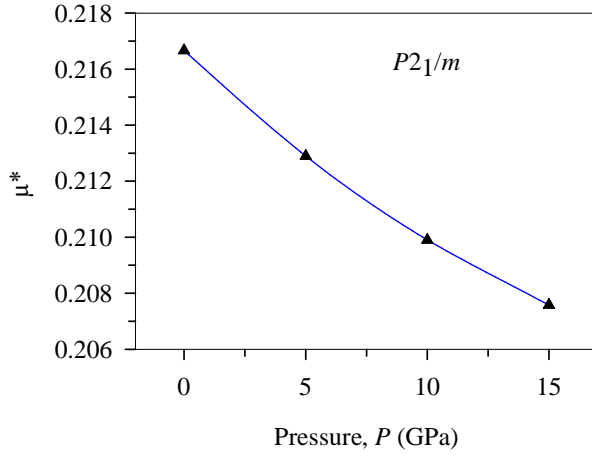
3.7 Superconducting properties

Zheng et al. [36] predicted superconductivity in the orthorhombic phase of MgVH_6 under pressure. They explored the electronic band structure, phonon spectrum, the Eliashberg function and superconducting transition temperature. The electron-phonon coupling constant was also estimated.

We have revisited the electronic band structures (not shown in this paper) of MgVH_6 in the orthorhombic and monoclinic structures over a wider pressure range. As far as superconductivity is concerned, the electronic energy density of states (DOS) at the Fermi level and the repulsive Coulomb pseudopotential are two important parameters [36,77-81]. It should be noted that MgVH_6 in the monoclinic phase is not superconducting [36]. Table 8 discloses the computed parameters related to superconductivity. For completeness, the electronic energy density of states at the Fermi level and the repulsive Coulomb pseudopotential of non-superconducting MgVH_6 in the monoclinic phase are also included in Table 8.

Table 8. DOS at the Fermi level $N(E_F)$ (States/eV), repulsive Coulomb pseudopotential μ^* , electron-phonon coupling constant λ , and T_c (K).

Space group	Crystal structure	Pressure P (GPa)	$N(E_F)$	μ^*	λ	T_c	Ref.
$P2_1/m$	Monoclinic	0	5.00	0.217	-	-	[This]
		5	4.52	0.213	-	-	
		10	4.19	0.210	-	-	
		15	3.96	0.208	-	-	
$Pmn2_1$	Orthorhombic	100	1.78	0.166	1.06	104.7	[This]
		125	1.50	0.156	0.89	53.8	
		150	1.27	0.145	0.75	34.9	
			2.40	0.10, 0.13	1.43	27.6, 25.0	[36]
		175	1.13	0.138	0.67	28.6	[This]
		200	1.07	0.134	0.63	26.1	



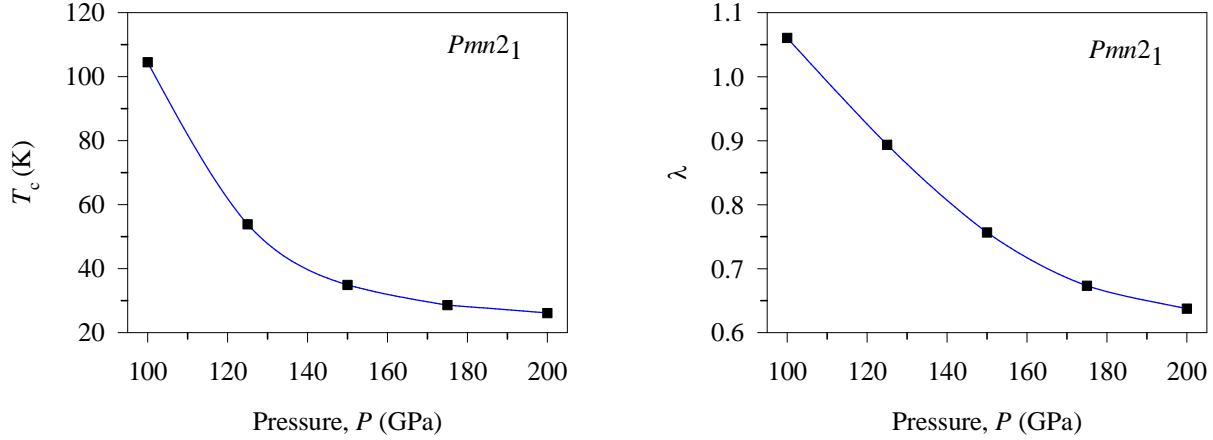


Figure 10: The repulsive Coulomb pseudopotential μ^* , electronic density of states at the Fermi level $N(E_F)$ (States/eV) (in both the phases), electron phonon coupling constant λ , and superconducting critical temperature T_c of MgVH_6 at different pressures in the orthorhombic structure only.

The McMillan equation given below is used to estimate T_c [82]:

$$T_c = \frac{\theta_D}{1.45} \exp \left[-\frac{1.04(1 + l)}{l - \mu^*(1 + 0.62l)} \right] \quad (15)$$

In Eqn. (15), λ is the electron-phonon coupling constant and μ^* is the repulsive Coulomb pseudopotential. The pressure variation in the electron-phonon coupling constant has been estimated following the procedure adopted in Ref. [78]. We have used the computed value of the λ from the Eliashberg spectral function at 150 GPa [36] as the reference value. In order to evaluate the pressure dependence of T_c , first, we need the pressure dependent variations of θ_D and $N(E_F)$ (since $\lambda = N(E_F)V_{e-ph}$, here V_{e-ph} is the electron-phonon coupling potential; a term which is a weakly varying function of pressure in most cases). The variations of $N(E_F)$, μ^* , λ , and T_c with pressure are shown in Fig. 10. The variations of θ_D as a function of pressure have been displayed in Fig. 9. In our calculations, the value of Coulomb pseudopotential, μ^* has been determined using the following equation [83]:

$$\mu^* = \frac{0.26 N(E_F)}{1 + N(E_F)} \quad (16)$$

The repulsive Coulomb pseudopotential is detrimental to the formation of Cooper pairs which is essential for superconductivity. High values of λ , θ_D , and low value of μ^* favor high-temperature superconductivity. From Table 8 it is observed that T_c decreases under pressure primarily due to the decrease in the DOS at the Fermi level. The DOS at the Fermi level is the dominant parameter known to affect T_c via electron-phonon coupling constant [77]. Our calculations, therefore, suggest that the change in the DOS at the Fermi level under pressure is the origin of the pressure dependence variations of T_c . Very large value of T_c of MgVH_6 at 100 GPa in the

orthorhombic structure results from an anomalously large value of the Debye temperature and relatively high value of the electronic energy density of states at the Fermi level. It is interesting to note that the DOS at the Fermi level is significantly higher in the non-superconducting monoclinic MgVH₆. At the same time, MgVH₆ in this structure has significantly lower Debye temperature and higher repulsive Coulomb pseudopotential compared to those in the orthorhombic structure.

3.8 Optical properties

The optical functions of MgVH₆ are evaluated for the two polarization directions [100] and [001] of incident photons up to 30 eV at different pressures. The overall pressure dependence is weak. In this section we show the representative results for 0 GPa for the *P2₁/m* and for 100 GPa for the *Pmn2₁* structures. The frequency/energy dependent dielectric function can be written as follows:

$$\varepsilon(\omega) = \varepsilon_1(\omega) + \varepsilon_2(\omega) \quad (17)$$

Here, ω is the angular frequency of the electromagnetic wave, and $\varepsilon_1(\omega)$ and $\varepsilon_2(\omega)$ are the real and imaginary parts of the dielectric functions. The imaginary part of dielectric functions can be expressed as follows [49,84]:

$$\varepsilon_2(\omega) = \frac{2\pi e^2}{\Omega \varepsilon_0} \sum_{k,v,c} |\psi_k^c| \mathbf{u} \cdot \mathbf{r} |\psi_k^v|^2 \delta(E_k^c - E_k^v - E) \quad (18)$$

Here, ω is the phonon angular frequency, e is the electronic charge, Ω is the unit cell volume, \mathbf{u} is the unit vector along the polarization of the incident electric field and ψ_k^c and ψ_k^v are the wave functions for conduction and valence band electrons at a particular value of k , respectively. In metallic solids the imaginary part of the dielectric constant comes from two contributions; inter-band and intra-band optical transitions. MgVH₆ in both the structures are metallic and, therefore, the intra-band transitions have crucial impact at the far infrared regions i.e., low energy part of the electromagnetic spectrum. To take account of the intraband transition for metallic material, the Drude damping correction is required [85,86]. Optical properties of MgVH₆ have been calculated considering screened plasma energy of 10 eV and a Drude damping of 0.08 eV.

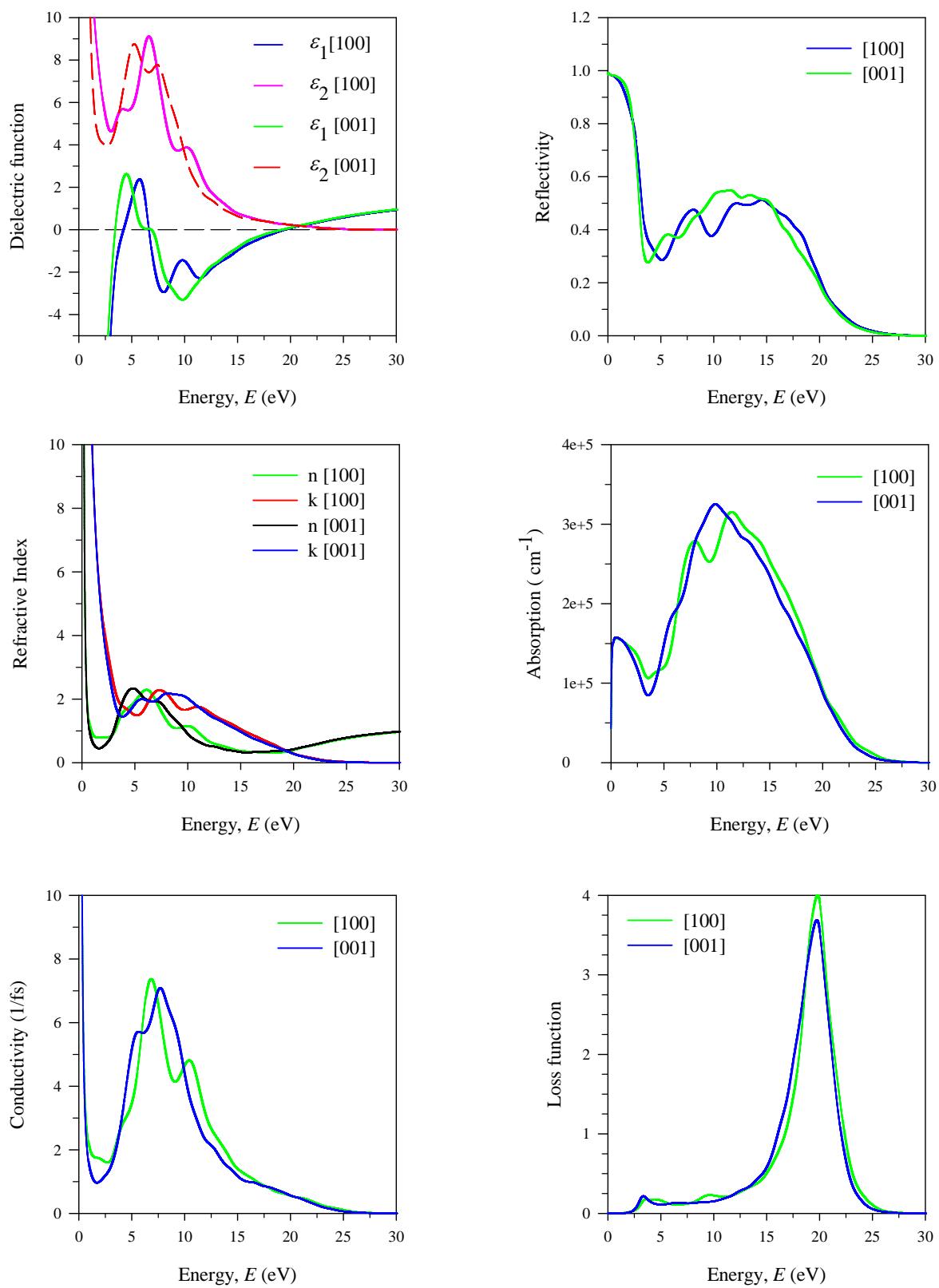


Figure 11: Optical properties of $(P2_1/m)$ MgVH₆ at 0 GPa.

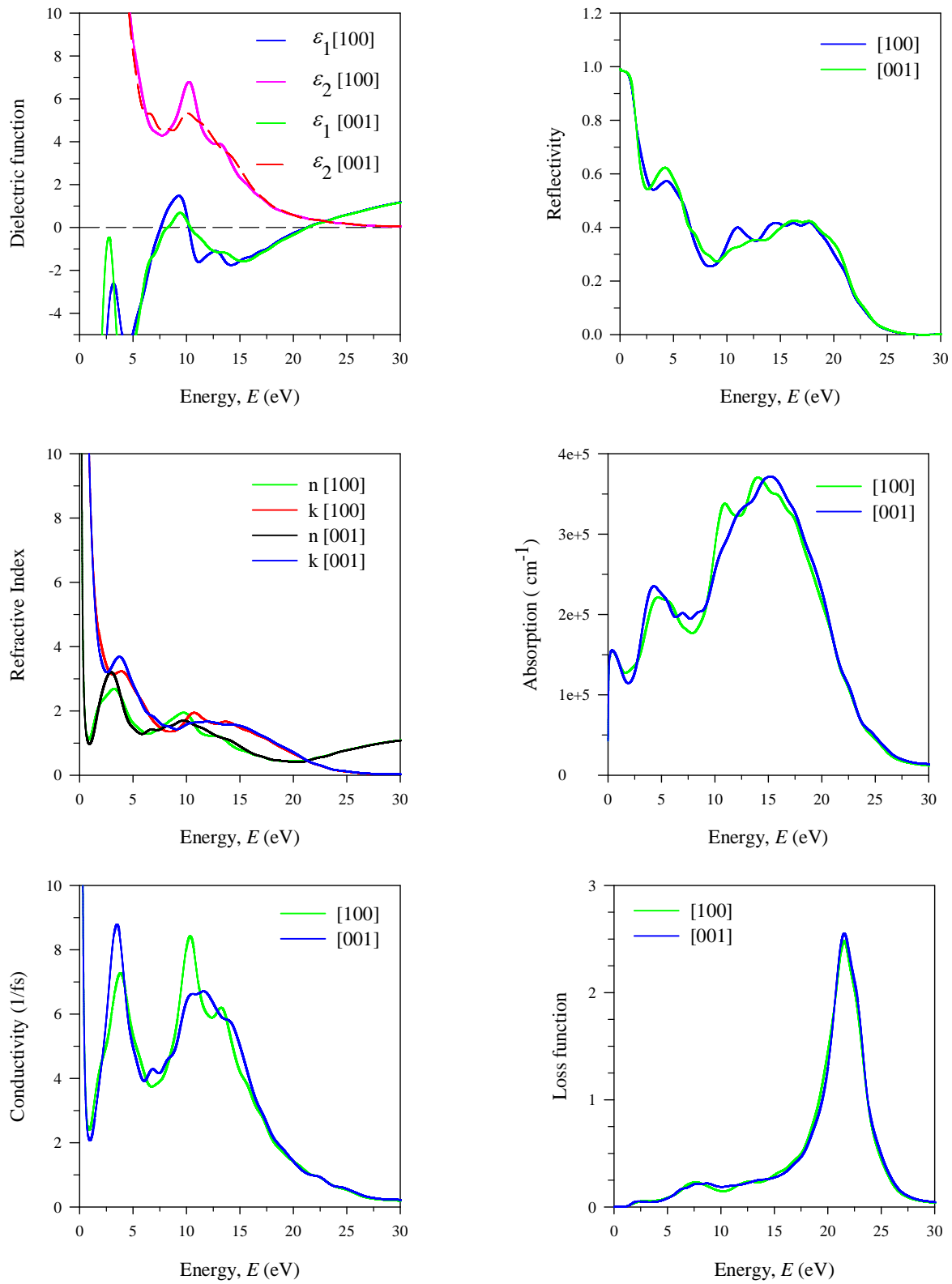


Figure 12: Optical properties of $(Pmn2_1) MgVH_6$ at 100 GPa.

Both real and imaginary parts of the dielectric function in monoclinic and orthorhombic structures show metallic character. The reflectivity is very high in the infra-red and visible regions of the electromagnetic spectra. According to Li et al. [85] a compound will be capable of reducing solar heating if it has a reflectivity $\sim 44\%$ in the visible light region. Therefore, MgVH_6 is a promising candidate for the practical usage as a coating material to avoid solar heating. The real part of the complex refractive index which determines the phase velocity of electromagnetic waves in MgVH_6 , is low in the visible region. The imaginary part, known as the extinction coefficient which measures the attenuation is high in the visible region. Both optical conductivity and absorption coefficient show metallic features. MgVH_6 is an efficient absorber of ultraviolet radiation. Loss function is a useful optical parameter describing the energy loss of a fast electron traveling in a material. The energy at which the loss function is a maximum is known as the plasma energy. The plasmons are excited and the reflectivity, absorption coefficient, and photoconductivity fall sharply at this energy. The material shows insulating behavior in response to incident photons above the plasma energy. The loss peaks are observed for $P2_1/m$ structure at 19.812 eV and 19.68 eV for the [100] and [001] electric field polarizations, respectively. For the $Pmn2_1$ structure, the loss peaks appear at the same energy, at 21.50 eV, for the [100] and [001] electric field polarizations. The optical anisotropy is low for MgVH_6 in both the structures.

4. Conclusions

DFT-based first-principles calculations have been carried out to find out the effects of hydrostatic pressure on the structural, elastic, thermophysical, superconducting state, and optical properties of MgVH_6 in the $P2_1/m$ and $Pmn2_1$ structures. The lattice parameters and unit cell volume decrease with pressure. The variation is systematic in the monoclinic phase but at high pressures the b - and c -axis lattice parameters show opposing trends. Both $P2_1/m$ and $Pmn2_1$ phases of MgVH_6 are thermodynamically stable. On the other hand, $P2_1/m$ phase of MgVH_6 is mechanically stable under the pressures considered here but the $Pmn2_1$ phase of MgVH_6 was found to be mechanically unstable under the pressures considered. Moreover, pressure variations of different elastic and thermophysical parameters indicate towards structural instability of MgVH_6 in the orthorhombic phase close to 100 GPa. For the $P2_1/m$ structure, both Poisson's ratio and Pugh's ratio are consistent with ductility. On the other hand, for the $Pmn2_1$ structure, the compound is predicted to be brittle at 100 GPa, and from 125 GPa – 200 GPa, it shows ductility. MgVH_6 in both the structures is elastically anisotropic. The hardness of MgVH_6 in the orthorhombic structure is very high at 100 GPa and falls sharply for further increase in pressure. The orthorhombic phase ($Pmn2_1$) has lower thermal expansion coefficient compared to that of monoclinic phase ($P2_1/m$). This also agrees with the elastic moduli, Debye temperature, and hardness values. The superconducting transition temperature decreases systematically with increasing pressure from a high value of 104.7 K at 100 GPa in the orthorhombic structure. This implies that a higher T_c might be achievable in the orthorhombic MgVH_6 ; the prime challenge here would be to ensure structural stability. The optical parameters are investigated in details.

Both the phases reveal clear metallic characters, high absorption capability of ultraviolet radiation and high reflectivity of infrared and visible light. Optical anisotropy is low in orthorhombic and monoclinic MgVH_6 .

Acknowledgements

S. H. N. acknowledges the research grant (1151/5/52/RU/Science-07/19-20) from the Faculty of Science, University of Rajshahi, Bangladesh, which partly supported this work.

Data availability

The data sets generated and/or analyzed in this study are available from the corresponding author on reasonable request.

Declaration of interest

The authors declare that they have no known competing financial interests or personal relationships that could have appeared to influence the work reported in this paper.

References

- [1] Mueller, W. M., Blackledge, J. P., & Libowitz, G. G. (Eds.). (2013). *Metal hydrides*. Elsevier.
- [2] Sakintuna, B., Lamari-Darkrim, F., & Hirscher, M. (2007). Metal hydride materials for solid hydrogen storage: a review. *International Journal of Hydrogen Energy*, 32(9), 1121-1140.
- [3] Mohtadi, R., & Orimo, S. I. (2016). The renaissance of hydrides as energy materials. *Nature Reviews Materials*, 2(3), 1-15.
- [4] Weast, R.C., Astle, M.J. and Beyer, W.H. (1984). *CRC Handbook of chemistry and physics*. CRC Press.
- [5] Reilly, J. J., & Wiswall, R. H. (1970). Higher hydrides of vanadium and niobium. *Inorganic Chemistry*, 9(7), 1678-1682.
- [6] Pedersen, A. S., & Larsen, B. (1993). The storage of industrially pure hydrogen in magnesium. *International Journal of Hydrogen Energy*, 18(4), 297-300.
- [7] Dehouche, Z., Goyette, J., Bose, T. K., & Schulz, R. (2003). Moisture effect on hydrogen storage properties of nanostructured MgH_2 -V-Ti composite. *International Journal of Hydrogen Energy*, 28(9), 983-988.
- [8] Zaluski, L., Zaluska, A., & Ström-Olsen, J. O. (1997). Nanocrystalline metal hydrides. *Journal of Alloys and Compounds*, 253, 70-79.
- [9] Zaluska, A., Zaluski, L., & Ström-Olsen, J. O. (1999). Nanocrystalline magnesium for hydrogen storage. *Journal of Alloys and Compounds*, 288(1-2), 217-225.

- [10] Gennari, F. C., Castro, F. J., Urretavizcaya, G., & Meyer, G. (2002). Catalytic effect of Ge on hydrogen desorption from MgH_2 . *Journal of Alloys and Compounds*, 334(1-2), 277-284.
- [11] Liang, G., Huot, J., Boily, S., Van Neste, A., & Schulz, R. (1999). Hydrogen storage properties of the mechanically milled MgH_2 -V nanocomposite. *Journal of Alloys and Compounds*, 291(1-2), 295-299.
- [12] Wang, H., Tse, J. S., Tanaka, K., Iitaka, T., & Ma, Y. (2012). Superconductive sodalite-like clathrate calcium hydride at high pressures. *Proceedings of the National Academy of Sciences*, 109(17), 6463-6466.
- [13] Gao, G., Oganov, A. R., Bergara, A., Martinez-Canales, M., Cui, T., Iitaka, T., & Zou, G. (2008). Superconducting high pressure phase of germane. *Physical Review Letters*, 101(10), 107002.
- [14] Xie, Y., Li, Q., Oganov, A. R., & Wang, H. (2014). Superconductivity of lithium-doped hydrogen under high pressure. *Acta Crystallographica Section C: Structural Chemistry*, 70(2), 104-111.
- [15] Zhou, D., Jin, X., Meng, X., Bao, G., Ma, Y., Liu, B., & Cui, T. (2012). Ab initio study revealing a layered structure in hydrogen-rich KH_6 under high pressure. *Physical Review B*, 86(1), 014118.
- [16] Wang, Z., Yao, Y., Zhu, L., Liu, H., Iitaka, T., Wang, H., & Ma, Y. (2014). Metallization and superconductivity of BeH_2 under high pressure. *The Journal of chemical physics*, 140(12), 124707.
- [17] Chen, X. J., Wang, J. L., Struzhkin, V. V., Mao, H. K., Hemley, R. J., & Lin, H. Q. (2008). Superconducting behavior in compressed solid SiH_4 with a layered structure. *Physical Review Letters*, 101(7), 077002.
- [18] Strobel, T. A., Somayazulu, M., & Hemley, R. J. (2009). Novel pressure-induced interactions in silane-hydrogen. *Physical Review Letters*, 103(6), 065701.
- [19] Gao, G., Hoffmann, R., Ashcroft, N. W., Liu, H., Bergara, A., & Ma, Y. (2013). Theoretical study of the ground-state structures and properties of niobium hydrides under pressure. *Physical Review B*, 88(18), 184104.
- [20] Li, Y., Gao, G., Xie, Y., Ma, Y., Cui, T., & Zou, G. (2010). Superconductivity at ~ 100 K in dense $\text{SiH}_4(\text{H}_2)_2$ predicted by first principles. *Proceedings of the National Academy of Sciences*, 107(36), 15708-15711.
- [21] Tse, J. S., Yao, Y., & Tanaka, K. (2007). Novel superconductivity in metallic SnH_4 under high pressure. *Physical Review Letters*, 98(11), 117004.
- [22] Drozdov, A. P., Eremets, M. I., Troyan, I. A., Ksenofontov, V., & Shylin, S. I. (2015). Conventional superconductivity at 203 kelvin at high pressures in the sulfur hydride system. *Nature*, 525(7567), 73-76.

- [23] Klein, B. M., & Cohen, R. E. (1992). Anharmonicity and the inverse isotope effect in the palladium-hydrogen system. *Physical Review B*, 45(21), 12405.
- [24] Ishizuka, M., Iketani, M., & Endo, S. (2000). Pressure effect on superconductivity of vanadium at megabar pressures. *Physical Review B*, 61(6), R3823.
- [25] Suzuki, N., & Otani, M. (2002). Theoretical study on the lattice dynamics and electron-phonon interaction of vanadium under high pressures. *Journal of Physics. Condensed Matter*, 14.
- [26] Drzazga, E. A., Domagalska, I. A., Jarosik, M. W., Szczyński, R., & Kalaga, J. K. (2018). Characteristics of superconducting state in vanadium: The Eliashberg equations and semi-analytical formulas. *Journal of Superconductivity and Novel Magnetism*, 31(4), 1029-1034.
- [27] Shi, L. T., Wei, Y. K., Liang, A. K., Turnbull, R., Cheng, C., Chen, X. R., & Ji, G. F. (2021). Prediction of pressure-induced superconductivity in the novel ternary system ScCaH_{2n} (n= 1–6). *Journal of Materials Chemistry C*, 9(23), 7284-7291.
- [28] Wei, Y. K., Jia, L. Q., Fang, Y. Y., Wang, L. J., Qian, Z. X., Yuan, J. N., & Wei, D. Q. (2021). Formation and superconducting properties of predicted ternary hydride ScYH₆ under pressures. *International Journal of Quantum Chemistry*, 121(4), e26459.
- [29] Li, D., Liu, Y., Tian, F. B., Wei, S. L., Liu, Z., Duan, D. F., & Cui, T. (2018). Pressure-induced superconducting ternary hydride H₃SXe: A theoretical investigation. *Frontiers of Physics*, 13(5), 1-9.
- [30] Ma, Y., Duan, D., Shao, Z., Li, D., Wang, L., Yu, H., & Cui, T. (2017). Prediction of superconducting ternary hydride MgGeH₆: From divergent high-pressure formation routes. *Physical Chemistry Chemical Physics*, 19(40), 27406-27412.
- [31] Liang, X., Bergara, A., Wang, L., Wen, B., Zhao, Z., Zhou, X. F., & Tian, Y. (2019). Potential high- T_c superconductivity in CaYH₁₂ under pressure. *Physical Review B*, 99(10), 100505.
- [32] Liang, X., Zhao, S., Shao, C., Bergara, A., Liu, H., Wang, L., & Tian, Y. (2019). First-principles study of crystal structures and superconductivity of ternary YSH₆ and LaSH₆ at high pressures. *Physical Review B*, 100(18), 184502.
- [33] Ma, Y., Duan, D., Shao, Z., Yu, H., Liu, H., Tian, F., & Cui, T. (2017). Divergent synthesis routes and superconductivity of ternary hydride MgSiH₆ at high pressure. *Physical Review B*, 96(14), 144518.
- [34] Song, P., Hou, Z., Baptista de Castro, P., Nakano, K., Hongo, K., Takano, Y., & Maezono, R. (2022). High-Pressure Mg–Sc–H Phase Diagram and Its Superconductivity from First-Principles Calculations. *The Journal of Physical Chemistry C*, 126(5), 2747-2755.

- [35] Zheng, J., Sun, W., Dou, X., Mao, A. J., & Lu, C. (2021). Pressure-driven structural phase transitions and superconductivity of ternary hydride MgVH₆. *The Journal of Physical Chemistry C*, 125(5), 3150-3156.
- [36] Jeon, K. J., Moon, H. R., Ruminski, A. M., Jiang, B., Kisielowski, C., Bardhan, R., & Urban, J. J. (2011). Air-stable magnesium nanocomposites provide rapid and high-capacity hydrogen storage without using heavy-metal catalysts. *Nature Materials*, 10(4), 286-290.
- [37] Pundt, A., & Kirchheim, R. (2006). Hydrogen in metals: Microstructural aspects. *Annual Review of Materials Research*, 36(1), 555-608.
- [38] Cheng, F., Tao, Z., Liang, J., & Chen, J. (2012). Efficient hydrogen storage with the combination of lightweight Mg/MgH₂ and nanostructures. *Chemical Communications*, 48(59), 7334-7343.
- [39] Feng, X., Zhang, J., Gao, G., Liu, H., & Wang, H. (2015). Compressed sodalite-like MgH₆ as a potential high-temperature superconductor. *RSC Advances*, 5(73), 59292-59296.
- [40] Lonie, D. C., Hooper, J., Altintas, B., & Zurek, E. (2013). Metallization of magnesium polyhydrides under pressure. *Physical Review B*, 87(5), 054107.
- [41] Sun, Y., Lv, J., Xie, Y., Liu, H., & Ma, Y. (2019). Route to a superconducting phase above room temperature in electron-doped hydride compounds under high pressure. *Physical Review Letters*, 123(9), 097001.
- [42] Arblaster, J. W. (2017). Thermodynamic properties of vanadium. *Journal of Phase Equilibria and Diffusion*, 38(1), 51-64.
- [43] Leupold, H. A., Iafrate, G. J., Rothwarf, F., Breslin, J. T., Edmiston, D., & AuCoin, T. R. (1977). Low-temperature specific heat anomalies in the group V transition metals. *Journal of Low Temperature Physics*, 28(3), 241-261.
- [44] Zhuang, Q., Jin, X., Lv, Q., Li, Y., Shao, Z., Liu, Z., & Cui, T. (2017). Investigation of superconductivity in compressed vanadium hydrides. *Physical Chemistry Chemical Physics*, 19(38), 26280-26284.
- [45] Li, X., & Peng, F. (2017). Superconductivity of pressure-stabilized vanadium hydrides. *Inorganic chemistry*, 56(22), 13759-13765.
- [46] Wang, Y., Lv, J., Zhu, L., & Ma, Y. (2010). Crystal structure prediction via particle-swarm optimization. *Physical Review B*, 82(9), 094116.
- [47] Wang, Y., Lv, J., Zhu, L., & Ma, Y. (2012). CALYPSO: A method for crystal structure prediction. *Computer Physics Communications*, 183(10), 2063-2070.
- [48] Kohn, W., & Sham, L. J. (1965). Self-consistent equations including exchange and correlation effects. *Physical Review*, 140(4A), A1133.

- [49] Clark, S. J., Segall, M. D., Pickard, C. J., Hasnip, P. J., Probert, M. I., Refson, K., & Payne, M. C. (2005). First principles methods using CASTEP. *Zeitschrift für Kristallographie-Crystalline Materials*, 220(5-6), 567-570.
- [50] Perdew, J. P., Burke, K., & Ernzerhof, M. (1996). Generalized gradient approximation made simple. *Physical Review Letters*, 77(18), 3865.
- [51] Vanderbilt, D. (1990). Soft self-consistent pseudopotentials in a generalized eigenvalue formalism. *Physical Review B*, 41(11), 7892.
- [52] Fischer, T. H., & Almlof, J. (1992). General methods for geometry and wave function optimization. *The Journal of Physical Chemistry*, 96(24), 9768-9774.
- [53] Monkhorst, H. J., & Pack, J. D. (1976). Special points for Brillouin-zone integrations. *Physical Review B*, 13(12), 5188.
- [54] Liu, Z. T. Y., Gall, D., & Khare, S. V. (2014). Electronic and bonding analysis of hardness in pyrite-type transition-metal pernitrides. *Physical Review B*, 90(13), 134102.
- [55] Liu, Z. T. Y., Zhou, X., Khare, S. V., & Gall, D. (2013). Structural, mechanical and electronic properties of 3d transition metal nitrides in cubic zincblende, rocksalt and cesium chloride structures: A first-principles investigation. *Journal of Physics: Condensed Matter*, 26(2), 025404.
- [56] Liu, Z. T. Y., Zhou, X., Gall, D., & Khare, S. V. (2014). First-principles investigation of the structural, mechanical and electronic properties of the NbO-structured 3d, 4d and 5d transition metal nitrides. *Computational Materials Science*, 84, 365-373.
- [57] Liu, Q. J., Ran, Z., Liu, F. S., & Liu, Z. T. (2015). Phase transitions and mechanical stability of TiO₂ polymorphs under high pressure. *Journal of Alloys and Compounds*, 631, 192-201.
- [58] Voigt, W. (1889). Ueber die Beziehung zwischen den beiden Elasticitätsconstanten isotroper Körper. *Annalen der Physik*, 274(12), 573-587.
- [59] Reuss, A. (1929). Berechnung der Fließgrenze von Mischkristallen auf Grund der Plastizitätsbedingung für Einkristalle. *Zeitschrift Angewandte Mathematik und Mechanik*, 9(1), 49-58.
- [60] Hill, R. (1952). The elastic behaviour of a crystalline aggregate. *Proceedings of the Physical Society. Section A*, 65(5), 349.
- [61] Frantsevich, I. N., Voronov, F. F., & Bakuta, S. A. (1982). Handbook on elastic constants and moduli of elasticity for metals and nonmetals. *Naukova Dumka*.
- [62] Pugh, S. F. (1954). XCII. Relations between the elastic moduli and the plastic properties of polycrystalline pure metals. *The London, Edinburgh, and Dublin Philosophical Magazine and Journal of Science*, 45(367), 823-843.

- [63] Ravindran, P., Fast, L., Korzhavyi, P. A., Johansson, B., Wills, J., & Eriksson, O. (1998). Density functional theory for calculation of elastic properties of orthorhombic crystals: Application to TiSi_2 . *Journal of Applied Physics*, *84*(9), 4891-4904.
- [64] Zhu, S., Zhang, X., Chen, J., Liu, C., Li, D., Yu, H., & Wang, F. (2019). Insight into the elastic, electronic properties, anisotropy in elasticity of manganese borides. *Vacuum*, *165*, 118-126.
- [65] Ranganathan, S. I., & Ostoja-Starzewski, M. (2008). Universal elastic anisotropy index. *Physical Review Letters*, *101*(5), 055504.
- [66] Schreiber, E., Anderson, O. L., Soga, N., & Bell, J. F. (1975). Elastic Constants and Their Measurement. *Journal of Applied Mechanics*, *42*(3), 747.
- [67] Ali, M. A., Hossain, M. M., Islam, A. K. M. A., & Naqib, S. H. (2021). Ternary boride Hf_3PB_4 : Insights into the physical properties of the hardest possible boride MAX phase. *Journal of Alloys and Compounds*, *857*, 158264.
- [68] Rano, B. R., Syed, I. M., & Naqib, S. H. (2020). Ab initio approach to the elastic, electronic, and optical properties of MoTe_2 topological Weyl semimetal. *Journal of Alloys and compounds*, *829*, 154522.
- [69] Teter, D. M. (1998). Computational alchemy: The search for new superhard materials. *MRS Bulletin*, *23*(1), 22-27.
- [70] Tian, Y., Xu, B., & Zhao, Z. (2012). Microscopic theory of hardness and design of novel superhard crystals. *International Journal of Refractory Metals and Hard Materials*, *33*, 93-106.
- [71] Chen, X. Q., Niu, H., Li, D., & Li, Y. (2011). Modeling hardness of polycrystalline materials and bulk metallic glasses. *Intermetallics*, *19*(9), 1275-1281.
- [72] El-Adawy, A., & El-KheshKhany, N. (2006). Effect of rare earth (Pr_2O_3 , Nd_2O_3 , Sm_2O_3 , Eu_2O_3 , Gd_2O_3 and Er_2O_3) on the acoustic properties of glass belonging to bismuth–borate system. *Solid State Communications*, *139*(3), 108-113.
- [73] Anderson, O. L. (1963). A simplified method for calculating the Debye temperature from elastic constants. *Journal of Physics and Chemistry of Solids*, *24*(7), 909-917.
- [74] Clarke, D. R. (2003). Materials selection guidelines for low thermal conductivity thermal barrier coatings. *Surface and Coatings Technology*, *163*, 67-74.
- [75] Mirzai, A., Ahadi, A., Melin, S., & Olsson, P. A. (2021). First-principle investigation of doping effects on mechanical and thermodynamic properties of Y_2SiO_5 . *Mechanics of Materials*, *154*, 103739.
- [76] Fine, M. E., Brown, L. D., & Marcus, H. L. (1984). Elastic constants versus melting temperature in metals. *Scripta Metallurgica*, *18*(9), 951-956.

- [77] Mridha, M. M., & Naqib, S. H. (2020). Pressure dependent elastic, electronic, superconducting, and optical properties of ternary barium phosphides (BaM_2P_2 ; M= Ni, Rh): DFT based insights. *Physica Scripta*, 95(10), 105809.
- [78] Khan, N. S., Rano, B. R., Syed, I. M., Islam, R. S., & Naqib, S. H. (2022). First-principles prediction of pressure dependent mechanical, electronic, optical, and superconducting state properties of NaC_6 : A potential high- T_c superconductor. *Results in Physics*, 33, 105182.
- [79] Islam, A. K. M. A., & Naqib, S. H. (1997). Possible explanation of high- T_c in some 2D cuprate superconductors. *Journal of Physics and Chemistry of Solids*, 58(7), 1153-1159.
- [80] Naqib, S. H. (2009). Modeling of the doping dependent superconducting transition temperatures for cuprates: Role of antiferromagnetic fluctuations. *Journal of Scientific Research*, 1(1), 14-21.
- [81] Shareef, S., Shamsuzzaman, A. M., Naqib, S. H., & Islam, A. K. M. A. (1999). Origin of doping dependence of transition temperature of $\text{La}_{2-x}\text{Ba}_x\text{CuO}_4$ in Van Hove singularity scenario. *Indian Journal of Pure and Applied Physics*, 37(2), 159-162.
- [82] McMillan, W. L. (1968). Transition temperature of strong-coupled superconductors. *Physical Review*, 167(2), 331.
- [83] Bennemann, K. H., & Garland, J. W. (1972). Theory for superconductivity in d-Band Metals. In *Superconductivity in d-and f-Band Metals*, 4, 103-137.
- [84] Alam, M. A., Shah, M. A. H., Nuruzzaman, M., Hadi, M. A., Parvin, F., & Zilani, M. A. K. (2021). Effect of hydrostatic compression on physical properties of Li_2TmSi_3 (Tm= Ir, Pt, Rh, Os) with ground-state optical features. *Journal of Physics and Chemistry of Solids*, 156, 110124.
- [85] Li, S., Ahuja, R., Barsoum, M. W., Jena, P., & Johansson, B. (2008). Optical properties of Ti_3SiC_2 and Ti_4AlN_3 . *Applied Physics Letters*, 92(22), 221907.
- [86] Wang, H., Chen, Y., Kaneta, Y., & Iwata, S. (2010). First-principles study on effective doping to improve the optical properties in spinel nitrides. *Journal of Alloys and Compounds*, 491(1-2), 550-559.

CRedit author statement

Md. Ashraful Alam: Methodology, Software, Formal analysis, Writing-Original draft. **F. Parvin:** Supervision, Writing-Reviewing and Editing. **S. H. Naqib:** Conceptualization, Supervision, Formal analysis, Writing- Reviewing and Editing.